Even harmonic pulse train generation by cross-polarization-modulation seeded instability in optical fibers

Julien Fatome, Ibrahim El Mansouri, Jean-Luc Blanchet, Stéphane Pitois, Guy Millot, Stefano Trillo, Stefan Wabnitz

Even harmonic pulse train generation by cross-polarization-modulation seeded instability in optical fibers

J. Fatome[1], I. El Mansouri[1], J.-L. Blanchet[1], S. Pitois[1], G. Millot[1], S. Trillo[2], and S. Wabnitz[1,3(a)]

1) Laboratoire Interdisciplinaire Carnot de Bourgogne, UMR 6303 CNRS/Université de Bourgogne, Dijon, France

2) Dipartimento di Ingegneria, Università di Ferrara, Via Saragat 1, 44122 Ferrara, Italy

3) Department of Information Engineering, Università di Brescia, Brescia, Italy

a) stefano.wabnitz@ing.unibs.it

Abstract: We show that, by properly adjusting the relative state of polarization of the pump and of a weak modulation, with a frequency such that at least one of its even harmonics falls within the band of modulation instability, one obtains a fully modulated wave at the second or higher even harmonic of the initial modulation. An application of this principle to the generation of a 80-GHz optical pulse train with high extinction ratio from a 40-GHz weakly modulated pump is experimentally demonstrated using a nonzero dispersion shifted fiber in the telecom C band.

OCIS codes:.(5530) Pulse propagation and temporal solitons; (4370) Nonlinear optics, fibers; (4380) Nonlinear optics, four wave mixing; (190) Nonlinear optics

1. Introduction

Modulation instability (MI) of a CW solution of the scalar nonlinear Schrödinger equation (NLSE) that describes pulse propagation in a weakly dispersive and nonlinear medium (e.g., an optical fiber) was first discovered by Bespalov and Talanov [1] for light waves in nonlinear liquids and by Benjamin and Feir for deep water waves [2], and extended to coupled wave models by Berkhoer and Zakharov [3] (for a recent review see also Ref. [4]). For scalar wave propagation, the MI-induced break-up of the CW in the anomalous group-velocity dispersion (GVD) leads to the formation of a train of pulses at the repetition rate set by the frequency of an initial modulation. Exact time-periodic solutions of the NLSE provide a full analytical description of the MI process past the initial stage of growth of the sidebands [5-7]. In a simpler approach most of the noteworthy features of the nonlinear stage of MI (e.g., the homoclinic structure) are also correctly captured by truncations to few Fourier modes [8-9]. A remarkable feature of the nonlinear dynamics of the MI process is that the wave evolution is generally periodic both in the time as well as in the propagation coordinate (the spatial periodicity is also referred to as Fermi-Pasta-Ulam recurrence), as also confirmed experimentally [10]. In the case of noise-activated MI, the modulation frequency which is selected corresponds to the peak of the gain curve corresponding to the nonlinear phase-matching. In the intermediate situation when multiple unstable modulations are present at the input, a nonlinear superposition of the periodic evolutions is obtained, which may lead to the generation of different pulse trains with harmonic frequencies at different points along the propagation coordinate [5, 7]. Indeed, it was numerically pointed out [11] and experimentally observed recently [12], that harmonic pulse trains may be generated at different distances even when a single sufficiently slow modulation is present at the

input. Seeding of these trains is produced by the generation of all of the harmonics at the point of maximum temporal compression of the pulse train at the fundamental frequency.

The most direct extension of the NLSE is provided by its vector counterpart or VNLSE where two polarization components are incoherently coupled via nonlinear cross-phase modulation. Such situation holds for instance in a birefringent fiber whenever the coherent terms can be averaged to zero by fast-rotating terms. In particular, in this case, the efficient conversion of a modulated wave into a nearly sinusoidally modulated wave at harmonic frequencies has been previously demonstrated by means of MI induced by multiple four-wave mixing in the case of a normally dispersive, highly birefringent fiber at visible wavelengths [13]. In this paper we rather focus on the VNLSE in the anomalous GVD regime, and in particular we are interested in the situation where the self- and cross-induced nonlinear terms have the same weight (Manakov system [14]), which applies to the relevant practical case of telecommunication fiber optic links with random birefringence [15]. MI for the VNLSE has been known for a long time [16], and its multiply periodic solutions representing the homoclinic extension of the unstable CW solutions have been obtained by methods based on the inverse scattering transform method [17-22]. These methods have also recently applied to obtaining deterministic rogue wave (or time and space localized) solutions of the VNLSEs, which may also be coupled with bright and dark soliton solutions [23-24].

In this work we point out and experimentally demonstrate an interesting and, to the best of our knowledge, yet unreported, property of the MI associated with polarized waves. Namely, whenever the CW and its modulation are orthogonally polarized at the input of an optical fiber, the projection of the initial modulation on the spatially unstable sidebands is initially zero so that no MI is activated at the fiber input. Nevertheless, MI is progressively induced upon propagation

on the CW through cross-polarization modulation (XPolM): as a result, the break-up of the CW into a pulse train is still observed. However with two important differences with respect to the scalar case, namely: (i) only even harmonics of the initial modulation are present in the pulse train; (ii) the CW pedestal that accompanies MI-induced pulse trains in the scalar case is fully suppressed in the vector case, thus permitting in principle to achieve very large extinction ratios. The application of this effect to the all-optical generation of a 80-GHz high-contrast pulse train from a cross-polarized 40-GHz electro-optical weak modulation is experimentally demonstrated.

2. Theory

The propagation of a polarized optical field in randomly birefringent optical fibers with relatively low polarization mode-dispersion (PMD) may be described in dimensionless units in terms of the VNLSE [9]

$$\begin{aligned} i\frac{\partial u}{\partial z}+\frac{1}{2}\frac{\partial^2 u}{\partial t^2}+\left(|u|^2+|v|^2\right)u=0 \\ i\frac{\partial v}{\partial z}+\frac{1}{2}\frac{\partial^2 v}{\partial t^2}+\left(|v|^2+|u|^2\right)v=0 \end{aligned} \qquad (1)$$

Here z and t denote the distance and retarded time (in the frame travelling at the common group-velocity) coordinates, respectively; whereas *u* and *v* indicate the two orthogonal polarization components of the field. Although we explicitly deal with the VNLSE in the integrable Manakov case, we point out that the phenomenon described below occurs for a generic ratio of the cross-to self-phase modulation coefficients as well. Let us consider the nonlinear evolution of a weakly modulated CW pump, which reads at z=0 as

$$\begin{aligned} u(z=0,t)=u_0+\varepsilon_u\exp(i\varphi_u)\cos(\Omega t) \\ v(z=0,t)=v_0+\varepsilon_v\exp(i\varphi_v)\cos(\Omega t), \end{aligned} \qquad (2)$$

where we take real carrier amplitudes u_0, v_0, with $u_0^2+v_0^2=1$; $\varepsilon_{u,v}$, $\phi_{u,v}$ and Ω are the initial modulation amplitudes, phases and frequency, respectively.

As it is well known, in the anomalous GVD regime MI of the CW solution of Eqs. (1) occurs for perturbations (2) with the same state of polarization of the pump (i.e., whenever $\phi_u=\phi_v$) and modulation frequency Ω in the range $0 \le \Omega \le \Omega_c$, where $\Omega_c=2$. The nonlinear evolution of the initial condition (2) leads to the development of a pulse train at the fundamental frequency Ω, that is with temporal period $T=2\pi/\Omega$. Such pulse train exhibits a spatial recurrent behavior in z, i.e., it periodically forms and then returns back to the initial CW along the propagation distance.

Moreover, whenever the harmonics of the initial modulation frequency (with, say, amplitude u_m for the m-th harmonic at frequency $m\Omega$) are also unstable (i.e., if $m\Omega \le \Omega_c$ with m>1), the nonlinear evolution of the weakly modulated pump (2) may also lead to the development of harmonic pulse trains, i.e. with periods $T_m=2\pi/(m\Omega)$. It is remarkable that these harmonic pulse trains typically appear at intermediate distances among the points of formation of the pulse trains at fundamental frequency Ω. In this way, by simply adjusting the input pump power one may select at the fiber output a particular repetition rate among the fundamental and its harmonics.

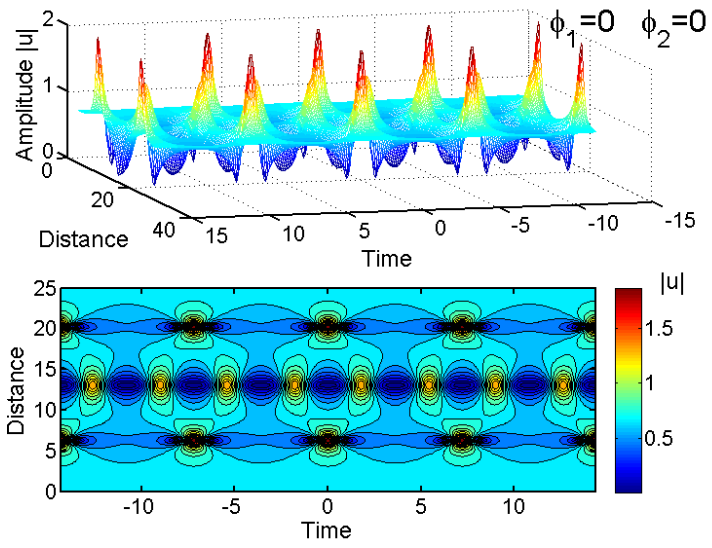

Fig.1 : Surface and contour plots of the evolution with distance of the field amplitude |u|. Initial in-phase amplitude modulation with $\Omega=\Omega_1=0.8718$, $\varepsilon_u=\varepsilon_v=10^{-2}u_0$, $\phi_u=\phi_v=0$.

The behavior of the solutions of the VNLSE reproduces the scalar situation in the case of input modulations with the same state of polarization of the pump. This is shown in Fig. 1 which displays the spatio-temporal evolution of the amplitude |u|, when the linearly polarized CW pump oriented at 45 degrees from the two degenerate axes of birefringence of the fiber (i.e., with $u_0^2=v_0^2=1/2$) is perturbed by an initial in-phase and parallel amplitude modulation with frequency Ω_1=0.8718 (so that $2\Omega_1<\Omega_c$) and $\varepsilon_u=\varepsilon_v=10^{-2}u_0$, $\phi_u=\phi_v$=0. As it can be seen from Fig.1, a primary pulse train with period T forms at approximately z=5 and z=20. At these distances, all harmonics of the fundamental frequency Ω are generated. Figure 1 also shows that near z=12 a harmonic secondary pulse train with period T_2 =T/2 is formed. Clearly, though the second harmonic 2Ω is absent in the input perturbation (2), such component is generated along the fiber whenever the fundamental pulse train is formed, as shown by Fig. 2a, which provides the evolution of the amplitude of the first four (positive) harmonics mΩ, m=1,2,3,4.

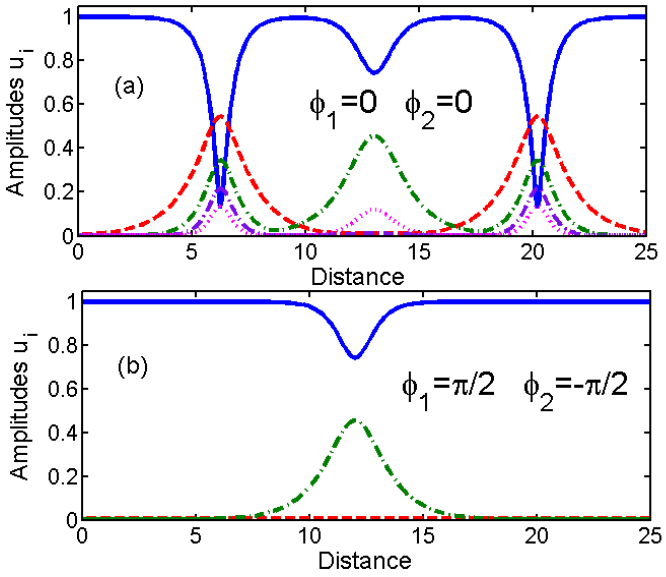

Fig. 2 : Evolution with distance z of the amplitudes of the pump and its harmonics u_i: (a) initial in-phase and parallel modulation, CW pump (blue solid curve), the sideband at frequency shift $\Omega=+\Omega_1$ from the pump (red dashed curve), its second harmonic at $\Omega=+2\Omega_1$ (green dot-dashed curve), third harmonic $\Omega=+3\Omega_1$ (violet dot-dashed curve), and fourth harmonic $\Omega=+4\Omega_1$ (pink dotted curve) corresponding to the case in Fig.1; (b) initial modulation orthogonal to the pump.

Note also from Fig. 2a that the secondary train is composed of even harmonics only. Because of the symmetry of the field spectrum about the pump carrier frequency, sidebands with opposite frequency detuning from the pump have equal amplitudes. The evolution of the orthogonal polarization component amplitude |v| is not reported here, since it is identical to |u|. The generation of the harmonic pulse train may be controlled by varying the relative phase between the CW pump and the input modulation: as it was shown in Ref. [11], with $\Omega=\Omega_1$ and in the case of quadrature modulation, that is whenever $\phi_u=\phi_v=\pi/2$, only the pulse train at the fundamental frequency is formed.

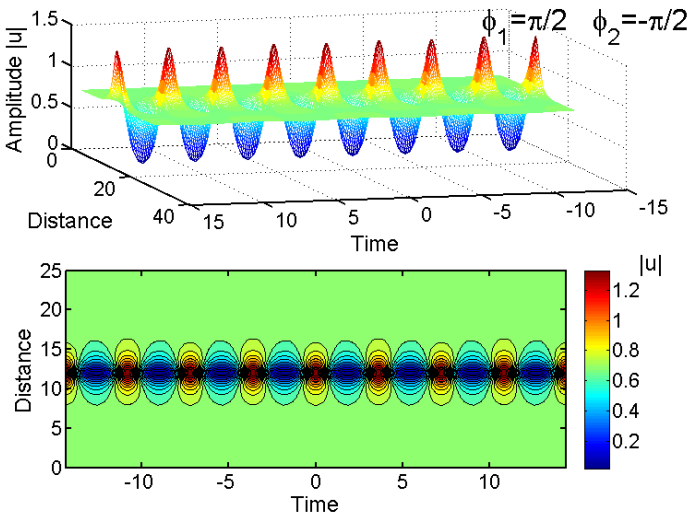

Fig. 3 : Same as Fig.1, with a quadrature modulation that is orthogonal to the pump, i.e., with $\phi_u = -\phi_v = \pi/2$.

The situation may be radically different in the case of input modulations with a different state of polarization from the pump. As it is shown in Fig. 2b and Fig. 3, for orthogonally polarized pump and sidebands ($\phi_u=-\phi_v=\pi/2$) the pulse train at the fundamental frequency $\Omega=\Omega_1$ is no longer generated: only a pulse train at the second harmonic frequency $2\Omega_1$ is observed. Again the evolution of the orthogonal amplitude |v| is the same as the evolution of |u| and is not reported here. Unlike the case of modulations with the same state of polarization as the pump, whenever the pump and the sidebands are orthogonally polarized the evolutions of the two polarization amplitudes are unaffected by their relative phase. In fact, the contour plot of the pulse amplitude |u| which is obtained with $\phi_u=0$, $\phi_v=\pi$ is the same as that of Fig. 3 where $\phi_u=-\phi_v=\pi/2$.

In order to better characterize the amplification process of the modulation in the crossed-polarized mode of the seed and its nonlinear evolution, we have numerically integrated Eqs. (1) with fixed modulation amplitude and phase $\phi_u=0$, $\phi_v=\pi$, by varying the value of the sideband frequency detuning Ω. The surface plot in Fig. 4a refers to a modulation frequency $\Omega=\sqrt{2}$,

which corresponds to peak MI gain for parallel modulations: as it can be seen, the MI gain vanishes for orthogonal modulations. Indeed, Fig. 4a shows that there is no exponential growth of the initial modulation. Conversely, only periodic small oscillations are observed. On the other hand, as shown in Figs. 4b-c, harmonic pulse trains at frequency 2Ω are always observed as soon as $\Omega \leq 1$, owing to the MI of the second harmonic of the initial modulation. Moreover, the modulation depth and the amplitude of the generated pulse train at the second-harmonic repetition rate grows larger as the sideband detuning is progressively reduced below Ω=1.

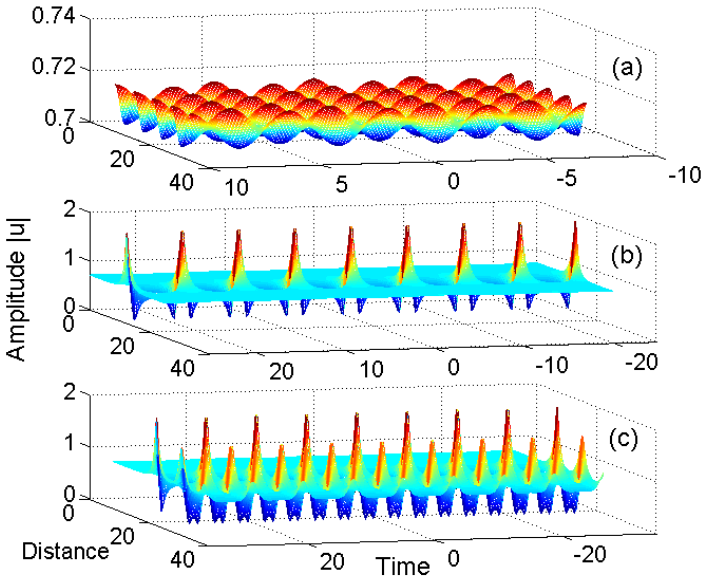

Fig. 4: Surface plot of the amplitude |u| with orthogonal input pump and sidebands ϕ_u =0, $\phi_v=\pi$, and the different sideband modulation frequencies: (a) $\Omega=\sqrt{2}$, (b) Ω=0.5 and (c) Ω=0.4.

As it can be seen from Fig. 5a, whenever Ω=0.5 the amplitude of the CW pump vanishes at the point of maximum pulse compression, which means that an ideal infinite extinction ratio is achieved. This can be explained as follows. In the theory of scalar nonlinear MI the normalized modulation frequency Ω=1 is the frequency which allows complete depletion of the pump towards the modulation and its harmonics. In fact, while a normalized modulation frequency

$\Omega=\sqrt{2}$ gives the maximum rate of conversion in the initial stage since it corresponds to nonlinear phase-matching, such rate is rapidly saturated by pump depletion which tends to drive the mixing interaction out of phase-matching (the new phase-matching frequency shifts towards lower frequencies). Conversely, a modulation with lower frequency, though being initially amplified at a lower rate, is progressively tuned towards nonlinear phase-matching by the pump depletion, the optimal condition corresponding indeed to a frequency Ω=1 [8, 9]. In the cross-polarization case examined here, this condition is realized when the second harmonic of the input modulation frequency is equal to Ω=1, which results indeed into an optimal input frequency Ω=0.5. In addition, Fig. 4c, 5b and 6b reveal that, whenever Ω<0.5, in addition to the second harmonic pulse train, a secondary pulse train is formed at the fourth harmonic frequency 4Ω, due to the parametric amplification owing to MI of the fourth harmonic. In particular, Fig. 6b shows that, for Ω=0.4, the second harmonic pulse train that is formed at around z=14 only contains even harmonics of the initial modulation, whereas the fourth harmonic pulse train that forms at z=23 only contains the fourth harmonic and its multiples.

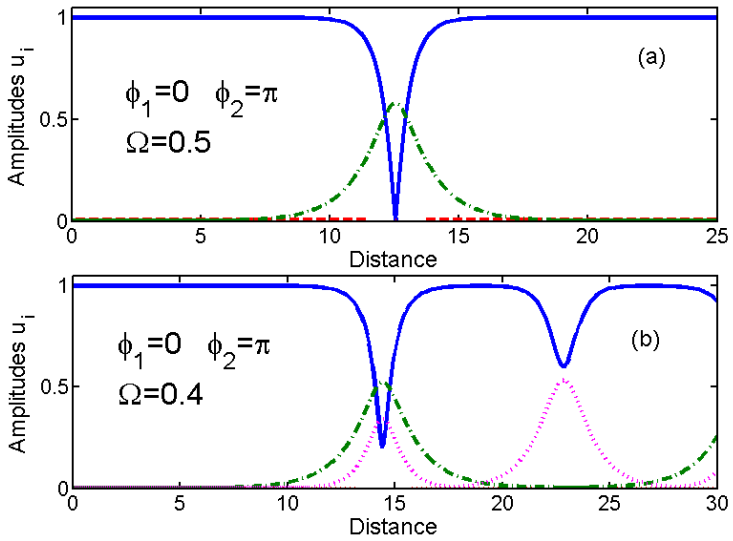

Fig. 5 : Same as in fig.2, with reference to the cases in fig.4 with (a) Ω=0.5 and (b) Ω=0.4.

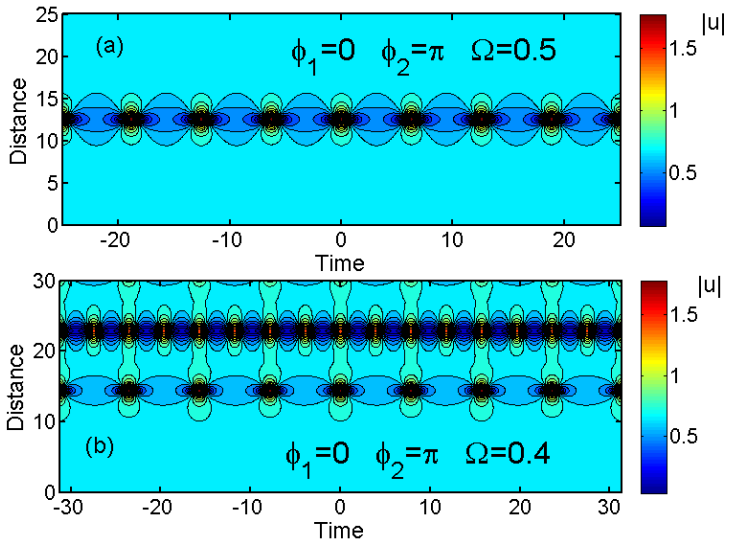

Fig. 6: Contour plots as in fig.5, with (a) Ω=0.5 and (b) Ω=0.4.

The physical mechanism that leads to the generation of pulse trains at repetition rates equal to even harmonics of the initial modulation is that orthogonal perturbations affect the CW pump propagation through cross-phase modulation, which implies that the perturbation acts on the pump through its squared modulus. Therefore nothing is expected to change with respect to previous cases if we rotate both the sidebands and the input pump linear polarization by π/4, so that we set in Eqs. (2) $u_0^2=1$, $v_0^2=0$, and $\varepsilon_u=0$, $\varepsilon_v=0.01$, $\phi_u=\phi_v=0$. The corresponding nonlinear evolution of the MI is shown in Fig. 7, where we display the surface plots of the amplitudes |u| and |v| of both polarization components of the field, with $\Omega=1/\sqrt{2}=0.707$. As expected, even though the initial modulation in Eq. (2) only involves sidebands at frequency Ω, also in this case even harmonics of the input modulation are created along the fiber by XPolM in the same polarization state of the pump wave.

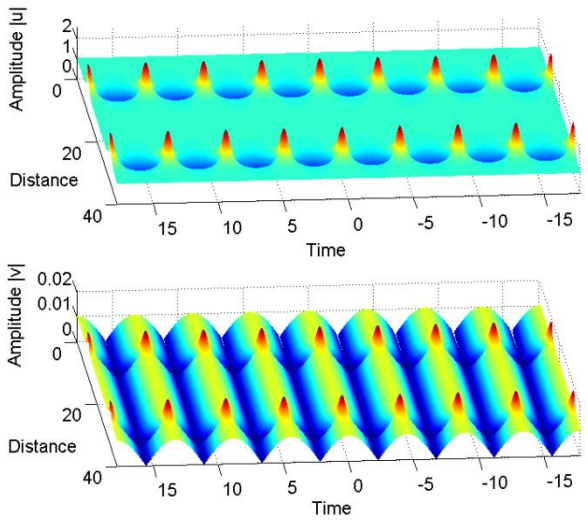

Fig. 7 : Surface plots of the temporal evolution with distance of the field amplitudes |u| and |v|, exhibiting recursive behavior. Input pump in the u mode (u_0=1, v_0=0) and modulation at frequency $\Omega = 1/\sqrt{2} = 0.707$ *in the v mode, ε_u=0, ε_v=10^{-2}, ϕ_u=ϕ_v=0. Note also the different vertical scale.*

This case allows us to get a deeper insight into the XPolM activated MI process. In fact, it might be surprising that new frequencies are generated onto mode u through a modulation impressed onto an orthogonal mode (v), which interacts only through the cross-phase modulation. In order to gain a better understanding of the underlying mechanisms, it is convenient to consider a finite-number mode truncation [9] by inserting in Eqs. (1) the expressions $u=u_0(z) + u_2(z) \exp(i\, 2\Omega\, t) + u_{-2}(z) \exp(-i2\, \Omega\, t)$ and $v= v_1(z) \exp(i\, \Omega\, t) + v_{-1}(z) \exp(-i\, \Omega\, t)$. By grouping terms of same frequency, one obtains a closed set of ODEs for the five Fourier modal amplitudes, which permits to isolate the mixing terms that are responsible for the generation of even harmonic frequency $(\omega_0 \pm 2\Omega)_u$ [henceforth the subscript indicates the mode to which the frequency belongs, while the frequency Ω within parenthesis is intended to be in real world units for dimensional consistency with the pump carrier frequency ω_0]. We find that

the latter are indeed generated as $(\omega_0+2\Omega)_u = (\omega_0+\Omega)_v - (\omega_0-\Omega)_v + (\omega_0)_u$ and $(\omega_0-2\Omega)_u = (\omega_0-\Omega)_v - (\omega_0+\Omega)_v + (\omega_0)_u$, which entails two independent photon processes: (i) a pair at $(\omega_0+2\Omega)_u$ and $(\omega_0-\Omega)_v$ is generated by annihilating a pair at $(\omega_0+\Omega)_v$ and $(\omega_0)_u$; (ii) a pair at $(\omega_0-2\Omega)_u$ and $(\omega_0+\Omega)_v$ is generated by annihilating a pair at $(\omega_0-\Omega)_v$ and $(\omega_0)_u$. Overall, the simultaneous occurrence of these two processes creates two photons in the even sidebands $(\omega_0 \pm 2\Omega)_u$ at the expense of two photons of the sole input pump at $(\omega_0)_u$, while leaving unchanged the number of photons in the orthogonal signal [i.e., $(\omega_0 \pm \Omega)_v$]. This description turns out to be consistent with the pure phase interaction between the pump mode u and the signal mode v. However, once the even modulation sidebands at $(\omega_0 \pm 2\Omega)_u$ are created through this double process, they are primarily amplified through the standard (scalar) mixing interaction which is behind seeded scalar MI, i.e., the direct generation of a photon pair at $(\omega_0+2\Omega)_u$ and $(\omega_0-2\Omega)_u$ at the expense of two photons at pump frequency $(\omega_0)_u$. This explains why the XPolM mechanism is only efficient when the normalized modulation frequency 2Ω falls within the bandwidth of scalar MI ($\Omega < 2$ in normalized units). At this point, we may also emphasize that such complicated multi-photon process could remarkably lead to the spatially periodic evolution of the amplification of even harmonic modulations, as it is shown in Fig. 7. In this sense, because of the competition between the XPolM and the scalar MI effects, the occurrence of XPolM-MI could also be viewed as a stabilization of the input pump against its decay into sideband pairs with the same polarization owing to spontaneous MI (i.e., due to amplification of noise). However, over long propagation distances (i.e. several spatial periods of the amplification of cross-polarized even harmonics, well beyond the length used in the experiment), the spontaneous MI of the pump is expected to hamper the recurrence of the seeded process, a problem which remains far beyond the scope of this paper and that will be addressed in details in a future study.

From the practical point of view, the interest of using cross-polarized sidebands in optical fibers is twofold. First of all, orthogonal modulations may be exploited whenever one wants to avoid the MI altogether. In fact, pump MI is fully suppressed as long as $\Omega \geq 1$ (as opposed to $\Omega \geq 2$ for the case of parallel sidebands). In addition, Fig.1 shows that even when $\Omega < 1$ the harmonic pulse train only develops after a distance which is more than twice the distance for the development of the fundamental pulse train. Thus if one wants to avoid MI, the limitation to the maximum fiber length (or pump power) is substantially mitigated. On the other hand, using cross-polarized sidebands leads to the possibility to impress a full modulation onto a CW laser at even multiples (2Ω-4Ω) of the initial frequency detuning Ω of the seed. By full modulation we mean that a large extinction ratio is obtained, thanks to the absence of the residual CW pedestal which always accompanies the fundamental pulse train generated by scalar MI, clearly visible in Fig. 2a. Note also from Fig.4c, 5b and 6b, that the quadrupling of the initial modulation frequency is observed at the relatively large distance z=23. This distance can be reduced substantially by increasing the relative strength of the initial modulation. See for example Fig. 8, where, as in Fig. 7, we have set in Eqs. (2) $u_0^2 = 1$, $v_0^2 = 0$, and $\varepsilon_u = 0$, $\phi_u = \phi_v = 0$, but we increased the orthogonal input modulation amplitude by ten times to have $\varepsilon_v = 0.1$: as it can be seen in Fig. 8, in this case frequency doubling is observed at z=8 (down from z=14 with $\varepsilon_v = 0.01$) and frequency quadrupling at z=14 (down from z=23 with $\varepsilon_v = 0.01$).

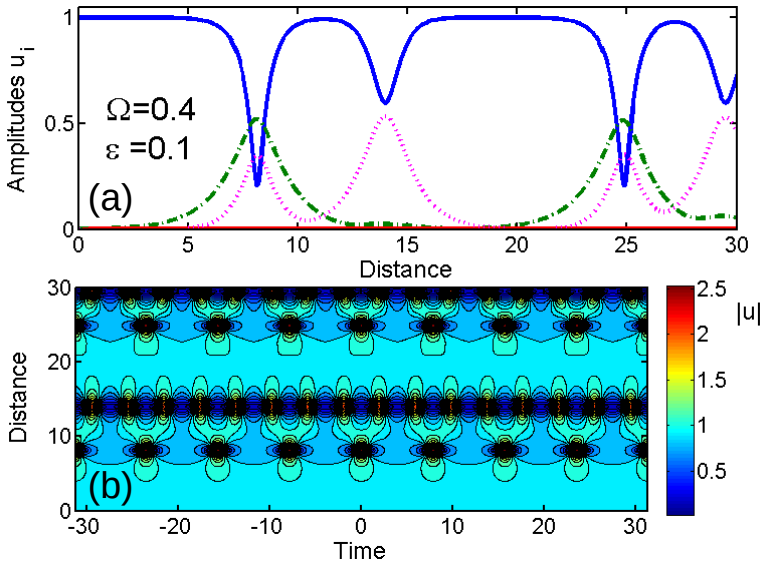

Fig. 8 : CW and sideband (a) amplitudes and (b) contour plot in the u mode with Ω= 0.4, ε_u=0, ε_v=10^{-1}, ϕ_u=ϕ_v=0.

By turning from dimensionless to real units, the input pump power P reads as $P=(\gamma Z_c)^{-1}$, where $\gamma = \omega n_2/(cA_{eff})$ is the fiber nonlinear coefficient, ω is the pump carrier frequency, n_2 is the nonlinear refractive index, and A_{eff} is the effective core area of the fiber. Moreover in Eqs.(1) $z=Z/Z_c$ and $t=T/T_c$, where Z and T are distance and time in real-world units, the dispersion length $Z_c=T_c^2/|\beta_2|$, $T_c=\Omega/(2\pi\Delta\nu)$, β_2 is the fiber chromatic dispersion at the pump frequency, and $\Delta\nu$ is the real-world frequency of the input modulation. For instance, taking the nonlinear coefficient of a highly nonlinear fiber γ=12 $W^{-1}km^{-1}$ and P=400 mW, one obtains Z_c=208 m, so that the distance z=14 as in Figs. (5-6) corresponds to an effective fiber length Z=2.9 km. With β_2=-12 ps^2/km one obtains T_c=1.6 ps, so that Ω=0.4 corresponds to $\Delta\nu$=40 GHz. In the following section we show that the observation of the phenomenon can also be carried out in dispersion-shifted low-PMD fiber with standard nonlinear coefficient.

3. Experiments

In this section we will confirm the theoretical predictions of the previous section, and experimentally show that one can produce a fully modulated periodic pulse train at the repetition rate of 80 GHz, that is well beyond the capabilities of electrically-driven modulators. The experimental setup is sketched in Figure 9. A continuous pump wave is generated by a laser diode emitting polarized light at 1555 nm. A first intensity modulator driven by a 40-GHz RF clock is then used to generate sidebands on either side of the pump frequency. Two of these sidebands will be used in the second part of this set-up to generate the sinusoidal signal wave.

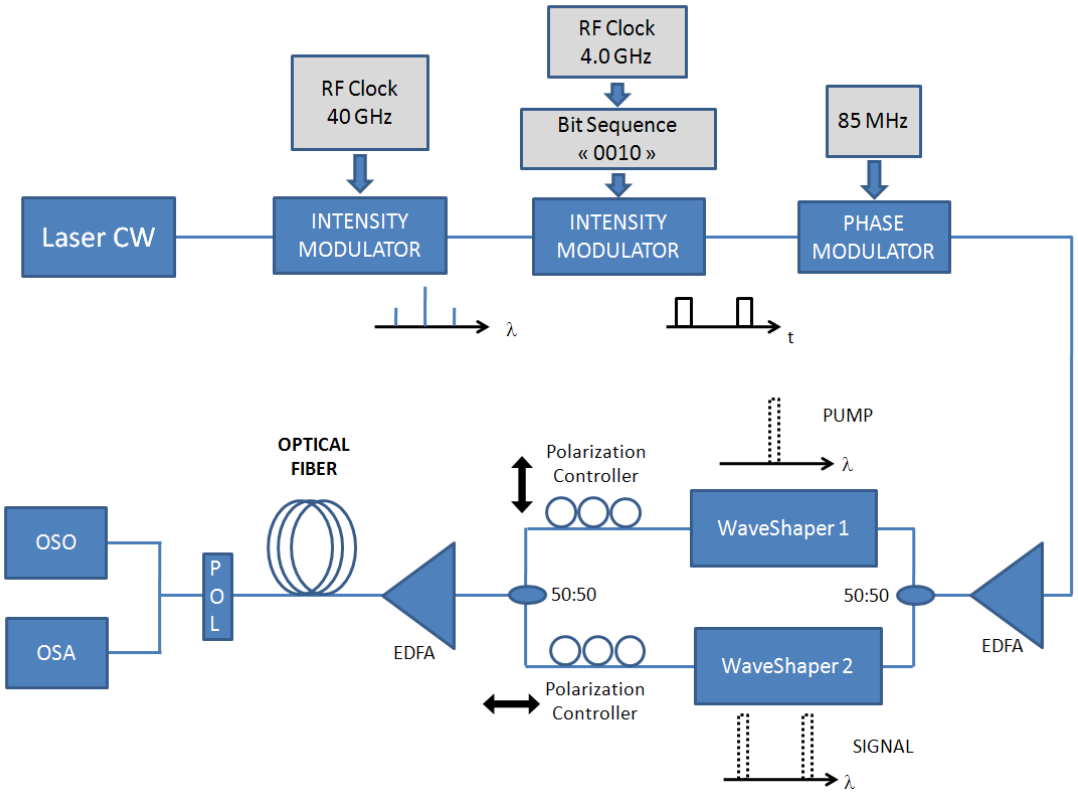

Fig. 9 : Experimental set up. EDFA: Erbium-Doped Fiber Amplifier. POL : polarizer. OSO: Optical Sampling Oscilloscope. OSA: Optical Spectrum Analyzer.

In order to inhibit the stimulated Brillouin scattering (SBS) effect that may occur in the optical fiber, a phase modulator is inserted into the setup so as to increase the spectral linewidth of the pump wave. The phase modulator is driven by a 28-dBm 85-MHz RF signal, thus enabling to work at relatively high pump powers, still being far below the SBS threshold. Moreover, in order to increase significantly the peak power involved in our experiment while keeping an average power below the SBS threshold, we have temporally carved the emitting light beam thanks to a second intensity modulator. More precisely, a 250-ps square pulse train at a repetition rate of 4 GHz (1/10 of the RF clock frequency of the first intensity modulator) is carved into the light beam thanks to a RF sequence of 4 bits (0010) so as to create a block of 10 initial signal periods with a duty cycle of 1:4. We would like to emphasize that such pulses provide a quasi-CW condition since the expected temporal modulation period will be around 12.5 ps. The light beam is then amplified and split owing to an EDFA and a 50:50 coupler, respectively. At this stage, pump and signal waves are spectrally separated by means of two programmable optical filters (Finisar Waveshaper) while their polarizations are independently adjusted by means of polarization controllers (PC) so as to emerge orthogonally (or parallel) polarized. Finally, pump and signal waves are re-combined before their amplification and injection into the optical fiber. The optical fiber used in our experiment was provided by Prysmian Group and has a length of 5100 m, a chromatic dispersion of D= 4.7 ps/nm/km, a dispersion slope S = 0.05 ps/nm^2/km and a nonlinear coefficient γ = 1.7 W^{-1}.km^{-1}. This fiber has a very low PMD equal to 0.02 ps/km$^{1/2}$. After propagation, the resulting signal was analyzed both in spectral and temporal domains by means of an Optical Spectrum Analyzer and a high bandwidth Optical Sampling Oscilloscope (EXFO PICOSOLVE), respectively.

In a first step, in order to experimentally determine the frequency at which the peak amplification of noise due the scalar MI (corresponding to peak gain of scalar MI or nonlinear phase-matching condition) is observed, only the pump wave is injected into the fiber. For a pump average power of 22 dBm (corresponding to 28 dBm peak power owing to the 1:4 duty cycle), our measurements show that the spontaneous scalar MI peaks at a frequency ν_{MI} = 82 GHz, consistently with the theoretical predictions obtained from the fiber parameters provided by the manufacturer.

In the second part of the experiment, pump and signal waves are injected into the fiber with parallel polarizations. The initial frequency modulation ν was fixed to about half of the scalar MI frequency ν H ν_{MI} / 2 = 40 GHz, determined in the first part of the experiment. The output spectral and temporal profiles are illustrated in Fig. 10 for a pump power of 19.7 dBm. As can be seen, and as predicted by the numerical calculations, one obtains a nearly triangular spectrum [see Fig. 10(b)], containing several harmonics of the initial modulation [25]. In the temporal domain [see Fig. 10(a)], one observes a compression of the initial sinusoidal beating, leading to the generation of pulses at a bit rate equal to the initial frequency modulation (40 GHz).

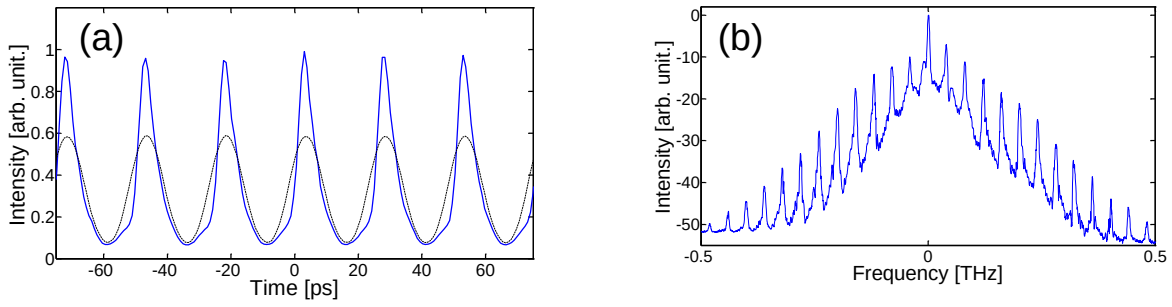

Fig. 10 : (a) Temporal profiles at the input (dashed line) and output (solid line) of the fiber when pump and signal waves have parallel polarization states (b) Experimental spectrum at the output of the fiber for input parallel polarized pump and signal and for a pump power of 19.7 dBm. Note that the output polarizer was oriented parallel to the pump polarization.

Finally, the pump and signal waves were injected into the fiber with orthogonal linear polarization states. The pump average power was fixed to 20.5 dBm whereas the signal power on the orthogonal axis was set to 10.5 dBm. The residual part of the signal wave on the pump axis was measured to be less than -6 dBm.

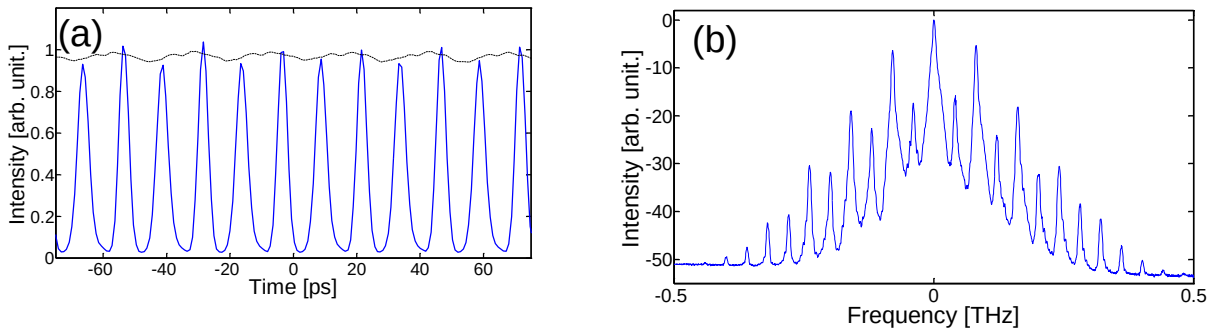

Fig. 11 : (a) Experimental temporal profiles at the input (dashed line) and output (solid line) of the fiber for orthogonal polarized pump and signal waves. (b) Corresponding output experimental spectrum. The output polarizer was oriented parallel to the pump polarization.

Figure 11(a) and (b) show the temporal and spectral profiles of the light wave at the output of the fiber when the analyzer was oriented parallel to the polarization of the emerging pump beam. As it can be seen, and contrary to the previous results shown in Figs. 10 obtained in the parallel polarizations case, the spectrum is now dominated by even harmonics at frequency k*80 GHz (k=1,2,…), whereas no exponential growth of the initial modulation is observed at 40 GHz. Indeed, in good agreement with the theoretical predictions of XPolM-MI in Section 2, the generation and amplification of the second harmonic of the modulation is obtained by using an initial frequency modulation fixed at about half of the peak gain frequency of scalar MI: $\Omega_{MI} / 2$ = 40 GHz. As illustrated in Fig. 11(a), in the temporal domain, this spectral feature is associated with the generation of a pulse train at twofold the initial signal frequency, corresponding to the

second-harmonic repetition rate of 80 GHz, in good qualitative agreement with the numerical predictions of Fig. 12, obtained from the numerical resolution of VNLSE. The experimental generated pulses have a nearly Gaussian shape with a temporal full width at half maximum of 4 ps. Note that the residual initial signal harmonics at 40 GHz and -40 GHz around -20 dBm, visible in Fig. 11(b), lead to a weak additional intensity modulation of the pulse train at a period of 25 ps.

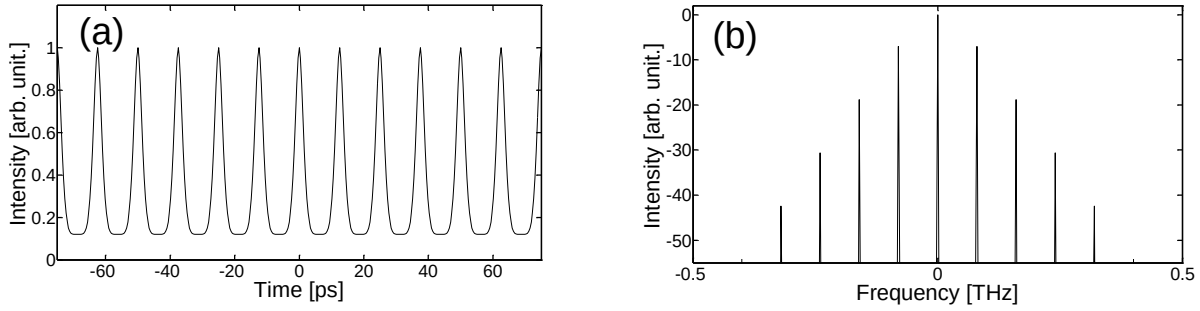

Fig. 12 : (a) Temporal and spectral profiles obtained from numerical simulations when the pump and signal waves are injected with orthogonal polarizations.

4. Conclusions

In this work we have theoretically predicted and experimentally demonstrated that, by using an orthogonally polarized pump and modulation signal at the input of a low-PMD, randomly birefringent optical fiber, only even harmonics of the modulation are amplified at the fiber output. Indeed, our experiments have shown the generation of a 80-GHz optical pulse train from a 40 GHz modulated signal in the telecom C band by using crossed pump and modulation using a nonzero dispersion shifted fiber.

This work was carried out with support from the Italian Ministry of University and Research (MIUR) through grant contract 2008MPSSNX and 2009P3K72Z, the Conseil Régional de Bourgogne, and the iXCore Foundation. We also thank Prysmian Group for providing the low PMD NZDSF fiber used in our experiment.

References

1. V. I. Bespalov and V. I. Talanov, "Filamentary structure of light beams in nonlinear liquids," Pis'ma Zh. Eksp. Teor. Fiz. **3**, pp. 471-476 (1966) [JETP Lett. **3**, pp. 307-310 (1966)].

2. T. B. Benjamin, J. E. Feir, "The disintegration of wave trains on deep water. Part 1: Theory," J. Fluid Mech., **27**, pp. 417 (1967).

3. L. A. L. Berkhoer and V. E. Zakharov, "Self excitation of waves with different polarizations in nonlinear media," Zh. Eksp. Teor. Fiz. **58**, 903-911 (1970) [Sov. Phys. JETP **31**, pp. 486-490 (1970)].

4. V. E. Zakharov and L.A. Ostrovsky, "Modulation instability: The beginning", Physica D **238**, 540-549 (2009).

5. N. N. Akhmediev, V. M. Eleonskii, N. E. Kulagin, "Generation of periodic trains of picosecond pulses in an optical fiber: exact solutions," Zh. Eksp. Teor. Fiz. **89, pp.** 1542-1551 (1985) [Sov. Phys. JETP, **62**, pp. 894-899 (1985)].

6. N. N. Akhmediev and V.I. Korneev, "Modulation instability and periodic solutions of the nonlinear Schrödinger equation," Teor. Mat. Fiz. 69, pp. 189 (1986) [Theor. Mat. Phys. 69, pp. 1089 (1986)].

7. N. N. Akhmediev, V. I. Korneev, and N. V. Mitskevich, "N-modulation signals in a single-mode optical waveguide under nonlinear conditions," Zh. Eksp. Teor. Fiz. **94**, 159-170 (1988) [Sov. Phys. JETP **67**, 89-95 (1988)].

8. G. Cappellini, and S. Trillo, "Third-order three-wave mixing in single-mode fibers: exact solutions and spatial instability effects," J. Opt. Soc. Am. B **8**, 824-838 (1991).

9. S. Trillo, and S. Wabnitz, "Dynamics of the nonlinear modulational instability in optical fibers," Opt. Lett. **16**, 986-988 (1991).

10. G. Van Simaeys, Ph. Emplit, and M. Haelterman, "Experimental Demonstration of the Fermi-Pasta-Ulam Recurrence in a Modulationally Unstable Optical Wave," Phys. Rev. Lett. **87**, 033902 (2001).

11. S. Wabnitz, N.N. Akhmediev, "Efficient modulation frequency doubling by induced modulation instability," Optics Communications **283**, 1152–1154 (2010).

12. M. Erkintalo, K. Hammani, B. Kibler, C. Finot, N.N. Akhmediev, J.M. Dudley, and G. Genty, "Higher-Order Modulation Instability in Nonlinear Fiber Optics," Phys. Rev. Lett. **107**, 253901 (2011).

13. G. Millot, "Multiple four-wave mixing-induced modulational instability in highly birefringent fibers," Opt. Lett. **26**, 1391-1393 (2001).

14. S. V. Manakov, "On the theory of two-dimensional stationary self-focusing of electromagnetic waves," Zh. Eksp. Teor. Fiz. **65**, 505-516 (1973) [Sov. Phys. JETP **38**, 248–253 (1974)].

15. P. K. A. Wai and C. R. Menyuk, "Polarization mode dispersion, decorrelation, and diffusion in optical fibers with randomly varying birefringence," J. Lightwave Technol. **14**, 148-157 (1996).

16. G. J. Roske, "Some nonlinear multiphase reactions," Stud. Appl. Math. **55**, 231–238 (1976).

17. M. Gregory Forest, S.P. Sheu, Otis C. Wright, "On the construction of orbits homoclinic to plane waves in integrable coupled nonlinear Schrödinger systems," Physics Letters A **266**, 24–33 (2000).

18. M. G. Forest, D. W. McLaughlin, D. J. Muraki, and O. C. Wright, "Nonfocusing Instabilities in Coupled, Integrable Nonlinear Schrödinger pdes," J. Nonlinear Sci. **10**, 291–331 (2000).

19. O. C. Wright, M.G. Forest, “On the Bäcklund-gauge transformation and homoclinic orbits of a coupled nonlinear Schrödinger system”, Physica D **141**, pp. 104–116 (2000).

20. M. G. Forest, O.C. Wright, “An integrable model for stable: unstable wave coupling phenomena, Physica D **178**, 173–189 (2003).

21. O. C. Wright, “The Darboux transformation of some Manakov systems,” Applied Math. Lett. **16**, pp. 647-652 (2003).

22. O. C. Wright III, “Dressing procedure for some homoclinic connections of the Manakov system,” Applied Math. Lett. **19**, 1185-1190 (2006).

23. B. Guo, L. Ling, “Rogue wave, breathers and bright-dark-rogue solutions for the coupled Schrödinger equations,” Chin. Phys. Lett. **28**, 110202 (2011).

24. F. Baronio, A. Degasperis, M. Conforti, S. Wabnitz, “Solutions of the Vector Nonlinear Schrödinger Equations: Evidence for Deterministic Rogue Waves,” Phys. Rev. Lett. **109**, 044102 (2012).

25. K. Hammani, B. Kibler, C. Finot, P. Morin, J. Fatome, J. M. Dudley, and G. Millot, “Peregrine soliton generation and breakup in standard telecommunications fiber,” Opt. Lett. **36**, 112-114 (2011).

Figure Captions

1. Surface and contour plots of the evolution with distance of the field amplitude |u|. Initial in-phase amplitude modulation with $\Omega=\Omega_1=0.8718$, $\varepsilon_u=\varepsilon_v=10^{-2}u_0$, $\phi_u=\phi_v=0$.

2. Evolution with distance z of the amplitudes of the pump and its harmonics u_i: (a) initial in-phase and parallel modulation, CW pump (blue solid curve), the sideband at frequency shift $\Omega=+\Omega_1$ from the pump (red dashed curve), its second harmonic at $\Omega=+2\Omega_1$ (green dot-dashed curve), third harmonic $\Omega=+3\Omega_1$ (violet dot-dashed curve), and fourth harmonic $\Omega=+4\Omega_1$ (pink dotted curve) corresponding to the case in Fig.1; (b) initial modulation orthogonal to the pump.

3. Same as fig.1, with a quadrature modulation that is orthogonal to the pump, i.e., with $\phi_u=-\phi_v=\pi/2$.

4. Surface plot of the amplitude |u| with orthogonal input pump and sidebands $\phi_u=0$, $\phi_v=\pi$, and the different sideband modulation frequencies: (a) $\Omega=\sqrt{2}$, (b) $\Omega=0.5$ and (c) $\Omega=0.4$.

5. Same as in fig.2, with reference to the cases in fig.4 with (a) $\Omega=0.5$ and (b) $\Omega=0.4$.

6. Contour plots as in fig.4, with (a) $\Omega=0.5$ and (b) $\Omega=0.4$.

7. Surface plots of the temporal evolution with distance of the field amplitudes |u| and |v|, exhibiting recursive behavior. Input pump in the u mode ($u_0=1$, $v_0=0$) and modulation at frequency $\Omega=1/\sqrt{2}=0.707$ in the v mode, $\varepsilon_u=0$, $\varepsilon_v=10^{-2}$, $\phi_u=\phi_v=0$. Note also the different vertical scale.

8. CW and sideband (a) amplitudes and (b) contour plot in the u mode with $\Omega=0.4$, $\varepsilon_u=0$, $\varepsilon_v=10^{-1}$, $\phi_u=\phi_v=0$.

9. Experimental set up. EDFA: Erbium-Doped Fiber Amplifier. POL : polarizer. OSO: Optical Sampling Oscilloscope. OSA: Optical Spectrum Analyzer.

10. (a) Temporal profiles at the input (dashed line) and output (solid line) of the fiber when pump and signal waves have parallel polarization states (b) Experimental spectrum at the output of the fiber for parallel polarized pump and signal and for a pump power of 19.7 dBm. Note that the output polarizer was oriented parallel to the pump polarization.

11. : (a) Experimental temporal profiles at the input (dashed line) and output (solid line) of the fiber for orthogonal polarized pump and signal waves. (b) Corresponding output experimental spectrum. The output polarizer was oriented parallel to the pump polarization.

12. (a) Temporal and spectral profiles obtained from numerical simulations when the pump and signal waves are injected with orthogonal polarizations.

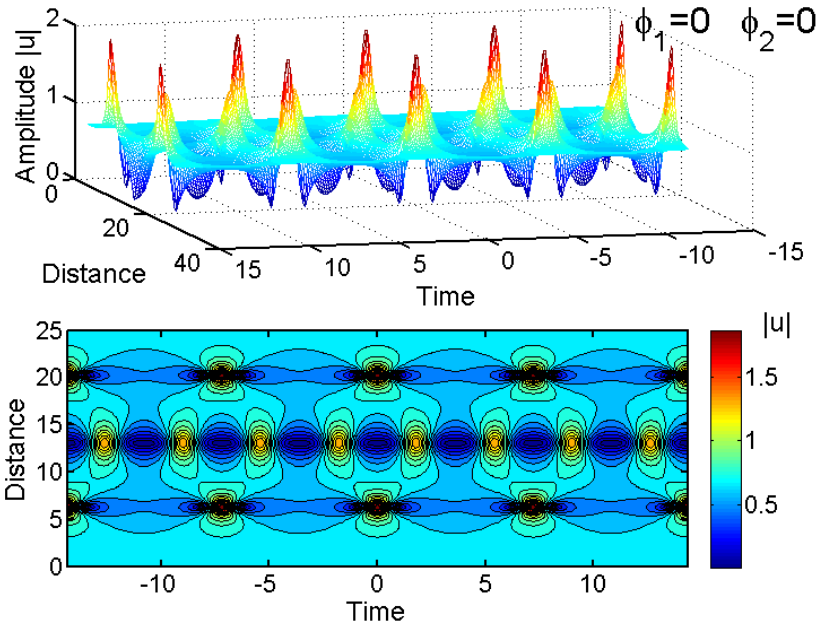

Figure 1

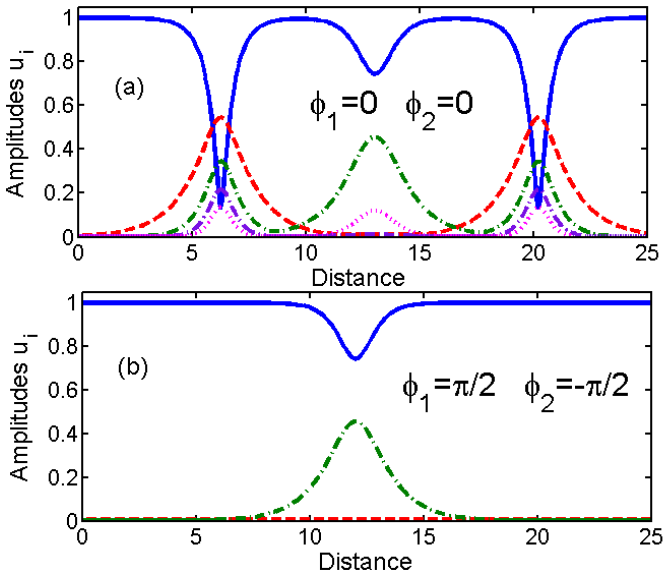

Figure 2

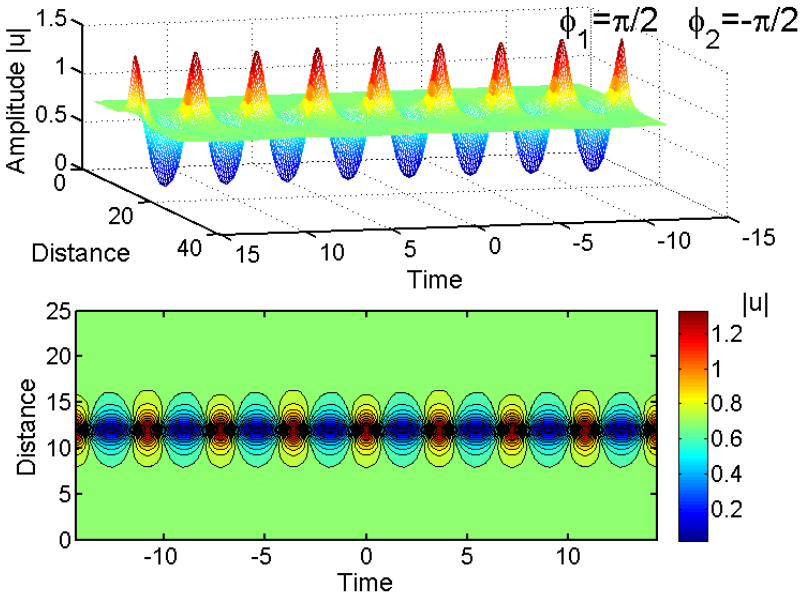

Figure 3

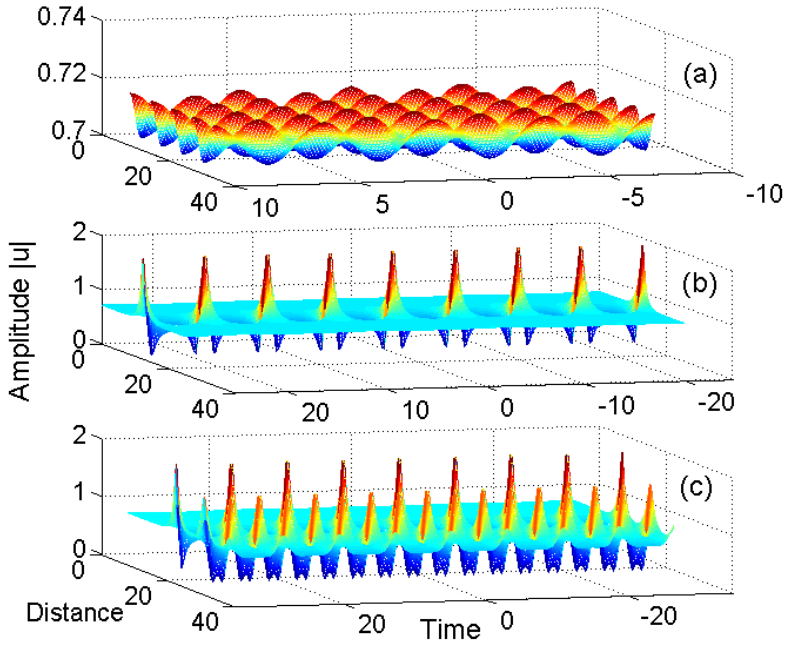

Figure 4

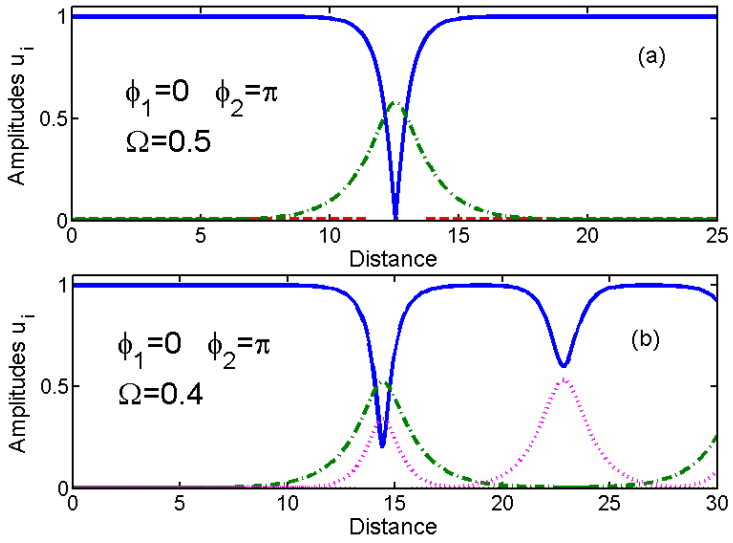

Figure 5

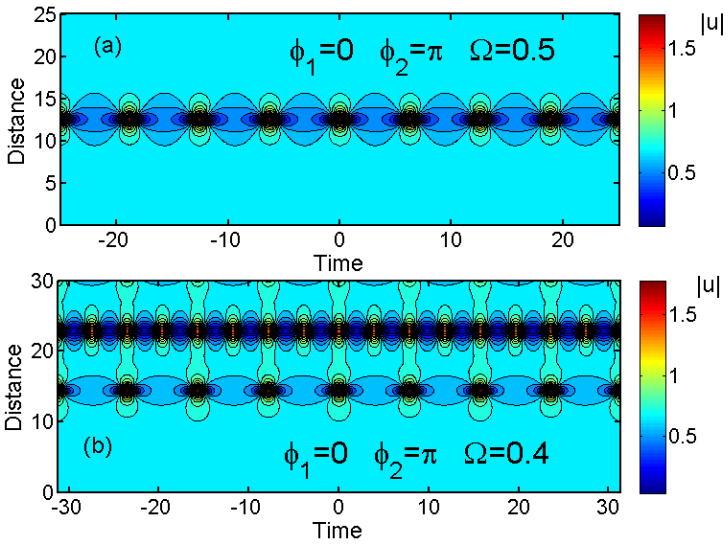

Figure 6

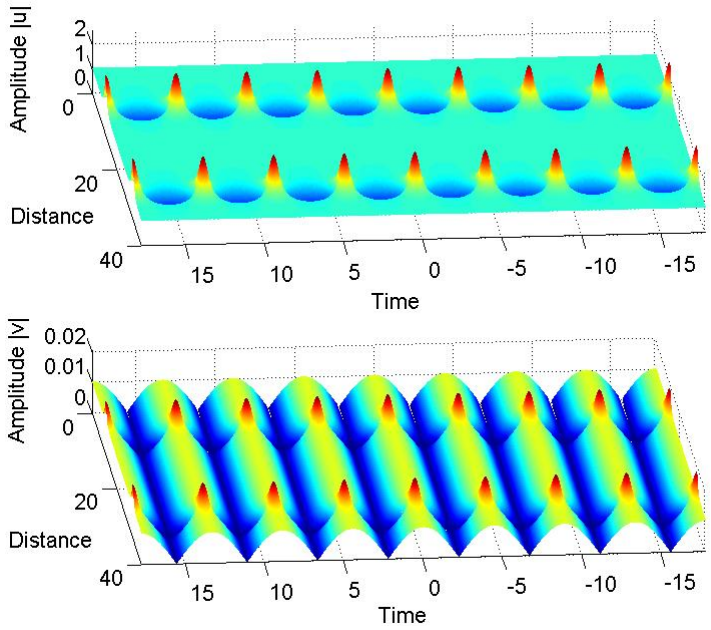

Figure 7

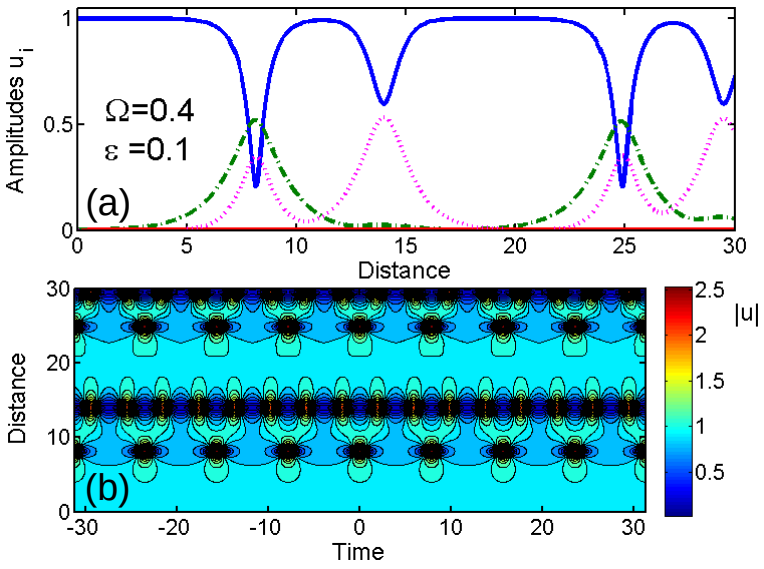

Figure 8

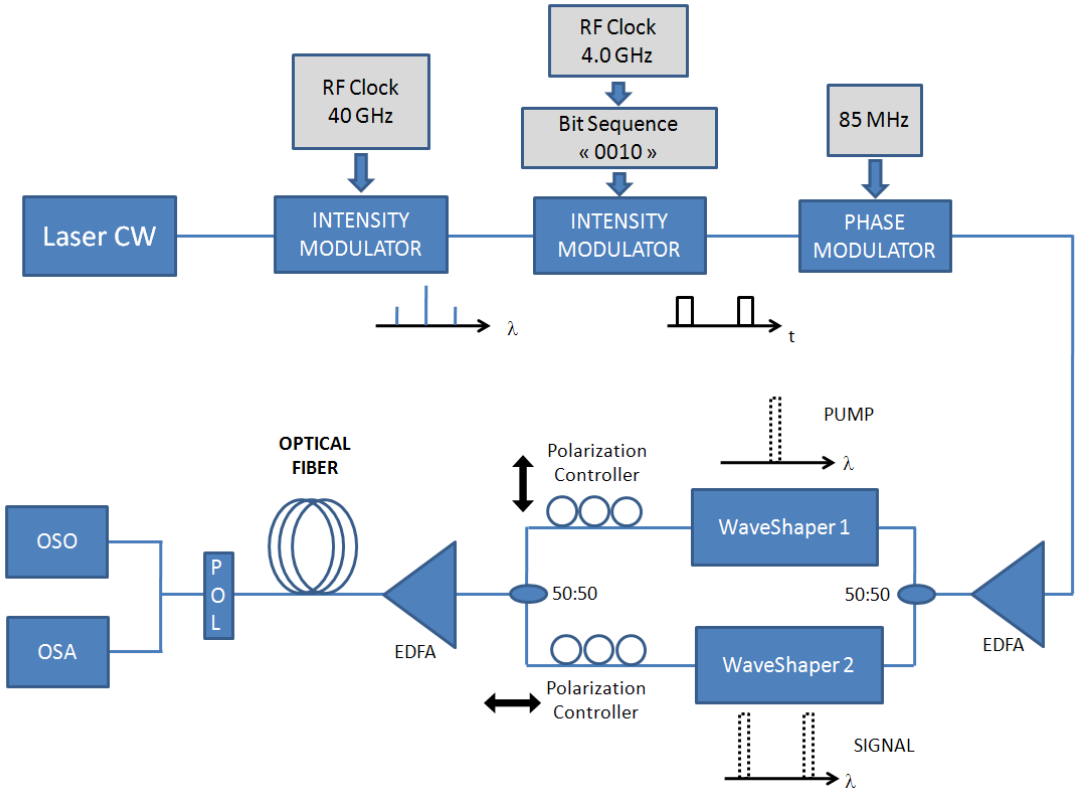

Figure 9

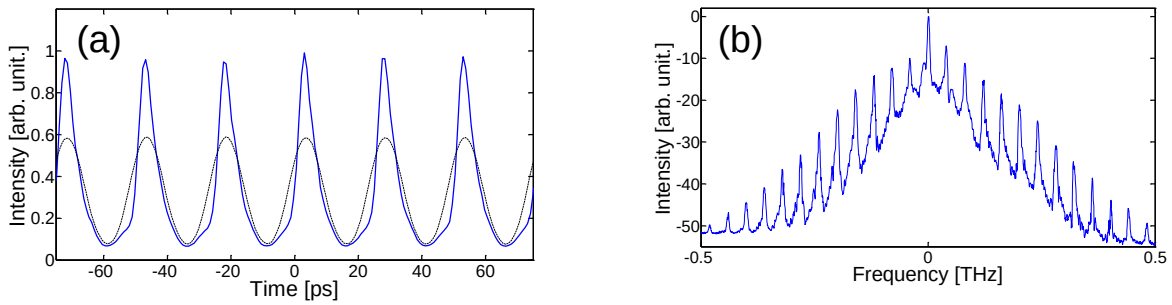

Figure 10

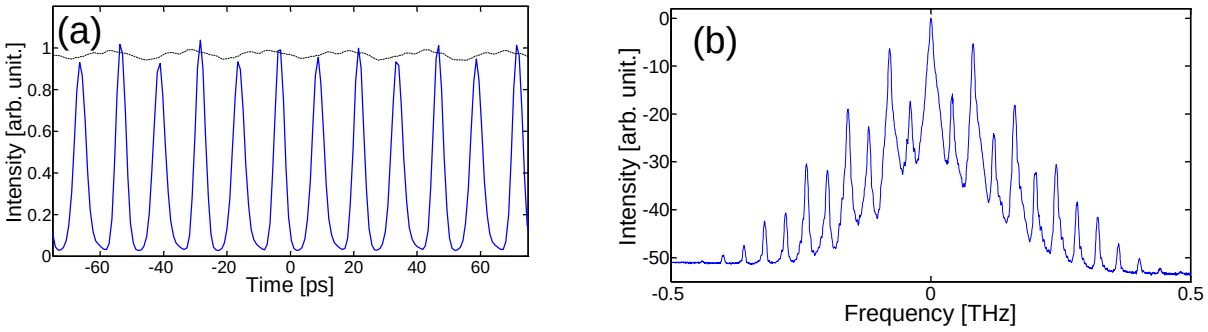

Figure 11

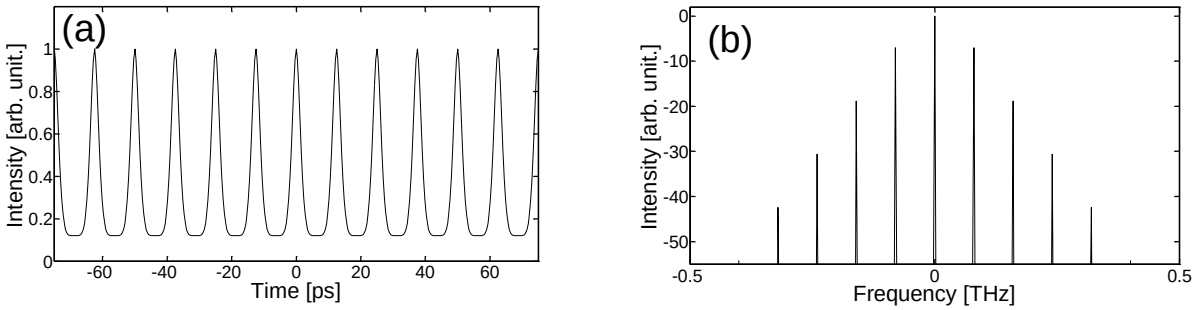

Figure 12